Chapter 5

Modeling and Control of Deformable Membrane Mirrors

Thomas Ruppel

Additional information is available at the end of the chapter

http://dx.doi.org/10.5772/52726

1. Introduction

The use of deformable mirrors (DMs) in adaptive optics (AO) systems allows for compensation of various external and internal optical disturbances during image aquisition. For example, an astronomical telescope equipped with a fast deformable secondary mirror can compensate for atmospheric disturbances and wind shake of the telescope structure resulting in higher image resolution [1–4]. In microscopy, deformable mirrors allow to correct for aberrations caused by local variations of the refractive index of observed specimen. Especially confocal and multi-photon microscopes particularly benefit from the improved resolution for visualization of cellular structures and subcellular processes [5, 6]. In addition, results of applied adaptive optics for detection of eye diseases and in vitro retinal imaging on the cellular level show promising examination and treatment opportunities [7–9].

In many AO systems, the deformable mirror is assumed to have negligible dynamical characteristics in comparison to the dynamic disturbances compensated by the deformable mirror. Unfortunately, this assumption is not always valid and active shape control of deformable mirrors must be employed to enhance the dynamic properties of the deformable mirror. For example, adaptive secondary mirrors for the Multi Mirror Telescope (MMT), the Large Binocular Telescope (LBT), and the Very Large Telescope (VLT) with diameters around 1 m have their first natural resonant frequencies below 10 Hz. In order to be able to use these systems for compensation of atmospherical disturbances with typical frequencies up to 100 Hz, active shape control is employed pushing the bandwith of these DMs to 1 kHz [10–13].

With up to 1170 voice coil actuators and co-located capacitive position sensors, the new generation of continuous face-sheet deformable mirrors requires fast and precise shape control. Thereby, the main idea for robust control of the mirror surface is the use of distributed voice coil actuators in combination with local position sensing by capacitive

sensors. The use of voice coil actuators allows for large stroke and exact positioning of the mirror while it is floating in a magnetic field. By changing the spatial properties of the magnetic field, the mirror shell can be deformed into a desired shape to compensate for optical aberrations measured by the AO system. Thereby, a low-contact bearing combined with little intrinsic damping of the mirror shell draws the need for adequate damping in closed loop operation. For the MMT deformable mirror, this problem is tackled by a 40 μm air-gap between the mirror shell and a reference plate behind the shell. The induced viscous damping is sufficient to operate the mirror within the designed specifications [11]. However, recent deformable mirrors for the LBT and VLT shall operate within a larger air-gap to provide more stroke. As a side effect, the requirement for a larger air-gap reduces the natural viscous damping and electronic damping is needed to achieve the same control bandwidth [14]. Therefore, the LBT and VLT type deformable secondary mirrors are controlled by local PD-control for each actuator/sensor pair in combination with feedforward force compensation [15]. Each actuator is driven by a dedicated local position controller running at 40-70 kHz. The shape command for the mirror unit is generated by a higher level wavefront control loop running at about 1 kHz. For small set-point changes of the mirror shell, this control concept is well-suited and has proven to be applicable in practice [16].

For high speed deformations over large amplitudes (e.g. chopping of deformable secondary mirrors), disadvantages of local PD-control must be considered. First of all, there is a shape-dependent stiffness and damping variation of the mirror shell. In particular, each deformation of the shell requires a specific amount of external force by the distributed actuators [11]. If local control instead of global control is used for position control of the shell, then robust and subsequently conservative controller design is necessary for all local control loops. Secondly, interaction of neighboring actuators has to be studied carefully. The control loop gains have to be chosen such that only little interaction with neighboring control loops is caused. Otherwise, the local control concept can lead to instability of the shell.

In order to further investigate practical concepts for DM shape control, there have been studies on MIMO optimal feedback control [17–19]. Certainly, the closed loop performance of a global optimal feedback control concept is superior to local PD-control. But still, the computational load of a global MIMO controller may not be suitable for large deformable mirrors with more than thousand actuators. Only in [17], the circular symmetry of the mirror shell is used to reduce the controllers complexity. Thereby, it is shown that symmetry can effectively reduce computational loads without loosing control performance. Although, even when symmetry is fully exploited, the computational effort for a global feedback control concept of future deformable mirrors is considerably high.

The most difficult task for control of deformable mirrors clearly is not the stabilization of the shell in a static shape, but changing the mirrors deflection in a predefined time and maintaining system stability. Instead of using a pure feedback controller for this task, model-based feedforward control concepts are proposed as in [20, 21]. In the past, the concept of model-based feedforward control has successfully been applied to various classes of dynamical systems. This technique is widely used in control practice as an extension of a feedback control loop to separately design tracking performance by the feedforward part and closed-loop stability and robustness by the feedback part. By using model-based feedforward control for shape control a deformable mirror, the feedback control loop is only needed to stabilize the shell in steady state and along precomputed trajectories. Thereby, the feedback loop can be designed to achieve high disturbance rejection. The computational load for feedforward control is comparably low because the feedforward signals may not be

http://dx.doi.org/10.5772/52726

computed in the feedback loop frequency (40-70 kHz for the LBT and VLT type DMs), but only when a new set-point is commanded (about 1 kHz for the LBT and VLT type DMs).

Since typical deformable mirrors do not significantly change their dynamical behavior over time, model-based time-invariant feedforward control can efficiently reduce load on implemented feedback controllers. Studies on model-based feedforward control of large deformable mirrors show that either with poorly tuned feedback control or even without feedback control, high speed and high precision deformations of deformable mirrors can be achieved [20, 21].[1] The required dynamical model of the DM can be identified based on internal position measurements of excited DM actuators. In [22], a practical identification procedure for small scale membrane DMs with static interferometric measurements and dynamic measurements from a laser vibrometer are presented, additionally. It is shown that together with an identified dynamical model, feedforward control can be employed for small scale membrane DMs also, significantly improving the settling time of the membrane mirror.

In the following, shape control of small and large deformable membrane mirrors by model-based feedforward and feedback control in a two-degree-of-freedom structure are described in a generalized framework. For this purpose, a scalable physical model of deformable membrane mirrors is derived based on force and momentum equilibriums of a differential plate element in Section 2. A series solution of the resulting homogeneous partial differential equation (PDE) is used to derive the modal coordinates of the inhomogeneous PDE including external actuator forces. This series solution can be employed to analyze and simulate the spatio-temporal behaviour of deformable mirrors and allows the design of a model-based shape controller in Section 4. The controller design section is devided into three parts. In Section 4.1, a trajectory generator for computation of differentiable reference trajectories describing the transient set-point change of the deformable mirror surface is described. In Section 4.2, a static and a dynamic feedforward controller are deduced from the inverse system dynamics of the mirror model, aftwards. Finally, a feedback controller is designed in Section 4.3 as a linear quadratic regulator based on a reduced dynamical mirror model in modal coordinates. After transforming the modal feedback controller into physical coordinates, its decentralized structure is implemented and its usability for future deformable mirrors is discussed.

2. Mirror modeling

Deformable membrane mirrors with non-contacting actuators are often represented by static models approximating the nonreactive deformation of the mirror surface. Thereby, both Kirchoff and van Kármán theory is used to describe plate deformations smaller than the plate thickness [23–26] and deformations close to the thickness of the mirror plate [27–29], respectively. Additionally, finite element methods are used to model deformable mirrors, in particular for the development large deformable secondary mirrors in astronomy [30–36]. In order to describe actuator influence functions, radially symmetric Gauss functions or splines are commonly used [2, 37], also. A more detailed static analysis is performed in [38] and [39] for a circularly clamped deformable mirror using a Kirchoff plate model. Additionally, in

[1] In this context, feedback control is mainly needed to account for model uncertainties and to reject external disturbances (e.g. mechanical vibrations, wind loads).

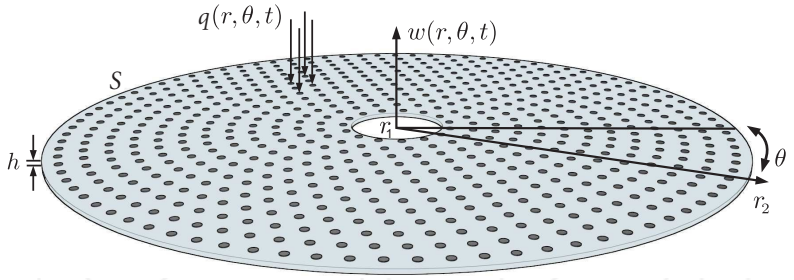

Figure 1. Schematics of a circular deformable mirror with deflection $w(r,\theta,t)$, inner radius r_1, outer radius r_2, plate thickness h, and external forces $q(r,\theta,t)$ acting on marked actuator positions over the mirror area S

[40] a deformable mirror with a free outer edge is modeled based on a Kirchoff plate model and resulting actuator influence functions for point forces are given.

Unfortunately, many of these modeling approaches only concentrate on the static characteristics of the deformable mirror and neglect dynamic properties like temporal eigenfrequencies and spatial characteristics of inherent eigenmodes. For model-based controller design addressed here, particularly these eigenfrequencies and eigenmodes are of substantial interest and can be found with the following modeling approach.

At first, circular deformable membrane mirrors with considerable out-of-plane stiffness and possible finite inner radius r_1 and outer radius r_2 centered at the origin of the $r-\theta$ plane are considered. Hereby, r,θ are polar coordinates. The plate is modelled as an isotropic Kirchoff plate with constant thickness h as shown in Figure 1.

For dynamic analysis, large deflections of the plate are not considered and nonlinear effects such as tensile stresses of the plate are neglected [28, 41, 42]. Secondly, it is assumed that a native curvature of the shell can be neglected due to only small deflections perpendicular to the surface.[2] The time varying deflection of the plate is measured by $w(r,\theta,t)$ relative to the undeflected reference and $t \in \mathbb{R}^+$ is the time. External forces caused by non-contacting voice coil actuators are represented by $q(r,\theta,t)$ and are defined by

$$q(r,\theta,t) = \sum_{m=1}^{M} \frac{1}{r_m} u_m(t)\delta(r-r_m)\delta(\theta-\theta_m), \tag{1}$$

where $u_m(t)$ corresponds to the actuator force at position (r_m,θ_m) and $\delta(r-r_m)\delta(\theta-\theta_m)$ describe the point-shaped force transmission.

The governing forces for a differential element of the plate are derived in Carthesian coordinates for simplicity. The differential element $h\mathrm{d}x\mathrm{d}y$ is effected by various shear forces, bending and twisting moments, and external loads as illustrated in Figure 2. The bending moments per unit length M_x, M_y arise from distributions of normal stresses σ_x,σ_y, while the twisting moments per unit length M_{xy},M_{yx} (shown as double-arrow vectors) arise from

[2] As discussed in [43], a possibly large radius of curvature and a large diameter of the deformable mirror spherical face-sheet (e.g. $2m$) in comparison to the considered deflections (usually around $100\mu m$) allows to approximate the spherical shell by a Kirchhoff plate. Similar assumptions are drawn in [44] for a comparable system.

http://dx.doi.org/10.5772/52726

shearing stresses τ_{xy}, τ_{yx}. The shear forces per unit length Q_x, Q_y arise from shearing stresses τ_{xz}, τ_{yz} [41].

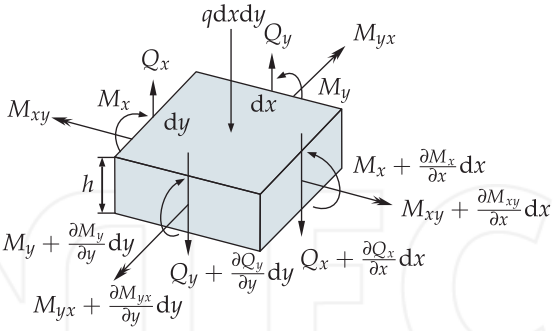

Figure 2. Illustration of shear forces, bending and twisting moments, and external loads affecting a differential plate element $h\mathrm{d}x\mathrm{d}y$ of the deformable mirror.

Of particular interest are the resulting three equations of motion

$$-Q_x\mathrm{d}y + \left(Q_x + \frac{\partial Q_x}{\partial x}\mathrm{d}x\right)\mathrm{d}y - Q_y\mathrm{d}x + \left(Q_y + \frac{\partial Q_y}{\partial y}\mathrm{d}y\right)\mathrm{d}x + q\mathrm{d}x\mathrm{d}y = \rho h\mathrm{d}x\mathrm{d}y\frac{\partial^2 w}{\partial t^2}, \tag{2a}$$

$$\left(M_y + \frac{\partial M_y}{\partial y}\mathrm{d}x\right)\mathrm{d}x - M_y\mathrm{d}x + M_{xy}\mathrm{d}y - \left(M_{xy} + \frac{\partial M_{xy}}{\partial x}\mathrm{d}x\right)\mathrm{d}y - Q_y\mathrm{d}x\mathrm{d}y = 0, \tag{2b}$$

$$\left(M_x + \frac{\partial M_x}{\partial x}\mathrm{d}x\right)\mathrm{d}y - M_x\mathrm{d}y - M_{yx}\mathrm{d}x + \left(M_{yx} + \frac{\partial M_{yx}}{\partial y}\mathrm{d}y\right)\mathrm{d}x - Q_x\mathrm{d}x\mathrm{d}y = 0, \tag{2c}$$

with $x, y, t \in \mathbb{R}$. Rotary-inertia effects of plate elements as well as higher-order contributions to the moments from loading q have been neglected in the moment equations (2b) and (2c). By canceling terms, the equations of motion reduce to

$$\frac{\partial Q_x}{\partial x} + \frac{\partial Q_y}{\partial y} + q = \rho h\frac{\partial^2 w}{\partial t^2}, \tag{3a}$$

$$\frac{\partial M_y}{\partial y} - \frac{\partial M_{xy}}{\partial x} - Q_y = 0, \tag{3b}$$

$$\frac{\partial M_x}{\partial y} + \frac{\partial M_{yx}}{\partial x} - Q_x = 0. \tag{3c}$$

By solving the last two equations for Q_x and Q_y and substituting in the first equation, a single equation in terms of various moments can be achieved reading

$$\frac{\partial^2 M_x}{\partial x^2} + \frac{\partial^2 M_{xy}}{\partial x\partial y} - \frac{\partial^2 M_{xy}}{\partial y\partial x} + \frac{\partial^2 M_y}{\partial y^2} + q = \rho h\frac{\partial^2 w}{\partial t^2}. \tag{4}$$

In [41], the relationship between the moments and the deflection is described and it is shown that the bending moments per unit length read

$$M_x = -D\left(\frac{\partial^2 w}{\partial x^2} + \nu\frac{\partial^2 w}{\partial y^2}\right), \tag{5a}$$

$$M_y = -D\left(\frac{\partial^2 w}{\partial y^2} + \nu\frac{\partial^2 w}{\partial x^2}\right), \tag{5b}$$

$$M_{xy} = -M_{yx} = D(1-\nu)\frac{\partial^2 w}{\partial x \partial y}, \tag{5c}$$

$$D = \frac{Eh^3}{12(1-\nu^2)}, \tag{5d}$$

with Young's modulus E and Poisson's ratio ν. By using the relationship $M_{xy} = -M_{yx}$ the biharmonic partial differentail equation (PDE)

$$D\left(\frac{\partial^4 w}{\partial x^4} + 2\frac{\partial^4 w}{\partial x^2 \partial y^2} + \frac{\partial^4 w}{\partial y^4}\right) - q = -\rho h\frac{\partial^2 w}{\partial t^2} \tag{6}$$

is derived.

Using (1) for a point actuated circular plate, Equation (6) can be written in polar coordinates as

$$D\nabla^4 w(r,\theta,t) + (\lambda_d + \kappa_d\nabla^4)\frac{\partial w(r,\theta,t)}{\partial t} + \rho h\frac{\partial^2 w(r,\theta,t)}{\partial t^2} = \sum_{m=1}^{M}\frac{u_m(t)}{r_m}\delta(r-r_m)\delta(\theta-\theta_m), \tag{7}$$

with the biharmonic operator ∇^4 given by

$$\nabla^4 = \nabla^2\nabla^2 = \left(\frac{\partial^2}{\partial r^2} + \frac{1}{r}\frac{\partial}{\partial r} + \frac{1}{r^2}\frac{\partial^2}{\partial\theta^2}\right)^2. \tag{8}$$

The parameters λ_d and κ_d are used to characterize additionally included viscous and Rayleigh damping and need to be identified in practice.

In order to fully describe the spatio-temporal behavior of deformable mirrors, the biharmonic equation (7) must be completed by physically motivated boundary conditions of the mirror plate. Typical boundary conditions for deformable mirrors are illustrated in Figure 3 (a)-(c) and can either be a clamped edge at $r = r_1$ reading

$$w(r_1,\theta,t) = 0 \tag{9a}$$

$$\frac{\partial w(r,\theta,t)}{\partial r}\Big|_{r=r_1} = 0, \tag{9b}$$

http://dx.doi.org/10.5772/52726

or a simply supported edge at $r = r_1$ reading

$$w(r_1, \theta, t) = 0 \tag{10a}$$

$$\frac{\nu}{r^2}\frac{\partial^2 w(r,\theta,t)}{\partial \theta^2} + \frac{\partial^2 w(r,\theta,t)}{\partial r^2} + \frac{\nu}{r}\frac{\partial w(r,\theta,t)}{\partial r}\Big|_{r=r_1} = 0\,, \tag{10b}$$

or a free edge at $r = r_1$ reading

$$\frac{\nu}{r^2}\frac{\partial^2 w(r,\theta,t)}{\partial \theta^2} + \frac{\partial^2 w(r,\theta,t)}{\partial r^2} + \frac{\nu}{r}\frac{\partial w(r,\theta,t)}{\partial r}\Big|_{r=r_1} = 0 \tag{11a}$$

$$\frac{(\nu-2)}{r^2}\frac{\partial^3 w(r,\theta,t)}{\partial r \partial \theta^2} - \frac{\partial^3 w(r,\theta,t)}{\partial r^3} + \frac{(3-\nu)}{r^3}\frac{\partial^2 w(r,\theta,t)}{\partial \theta^2} - \frac{1}{r}\frac{\partial^2 w(r,\theta,t)}{\partial r^2} + \frac{1}{r^2}\frac{\partial w(r,\theta,t)}{\partial r}\Big|_{r=r_1} = 0. \tag{11b}$$

In order to include a flexible support at $r = r_1$ (see Figure 3 (d)), boundary conditions (11) can be extended by a righting moment c reading

$$-c\frac{\partial w(r,\theta,t)}{\partial r} + \frac{\nu}{r^2}\frac{\partial^2 w(r,\theta,t)}{\partial \theta^2} + \frac{\partial^2 w(r,\theta,t)}{\partial r^2} + \frac{\nu}{r}\frac{\partial w(r,\theta,t)}{\partial r}\Big|_{r=r_1} = 0, \tag{12a}$$

$$\frac{(\nu-2)}{r^2}\frac{\partial^3 w(r,\theta,t)}{\partial r \partial \theta^2} - \frac{\partial^3 w(r,\theta,t)}{\partial r^3} + \frac{(3-\nu)}{r^3}\frac{\partial^2 w(r,\theta,t)}{\partial \theta^2} - \frac{1}{r}\frac{\partial^2 w(r,\theta,t)}{\partial r^2} + \frac{1}{r^2}\frac{\partial w(r,\theta,t)}{\partial r}\Big|_{r=r_1} = 0. \tag{12b}$$

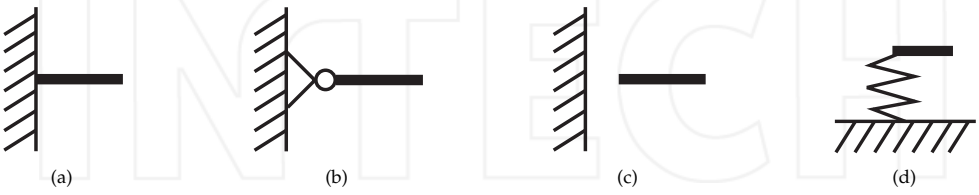

Figure 3. Schematics of four typical boundary conditions for deformable membrane mirrors showing (a) a clamped edge, (b) a simply supported edge, (c) a free edge, and (c) a spring supported edge type.

The PDE (7) and the boundary conditions (9)-(11) fully describe both the temporal and the spatial behavior of the modelled deformable mirror. In order to quantify the resulting eigenfrequencies and eigenfunctions for a given mirror geometry and material properties, the PDE will be analyzed further in the following section.

3. Fundamental solution and modal analysis

One way to analyze PDE (7) is to discretize the PDE in its spatial coordinates (r, θ). Thereby, the spatial differential operator ∇^4 and the boundary conditions (9)-(11) can be approximated by finite difference or finite element methods and the PDE is reduced to a finite set of coupled ordinary differential equations (ODE). The Eigenfrequencies and the eigenvectors of the resulting generalized eigenvalue problem correspond to the spatially discretized eigenfunctions of the PDE. Thereby, the spatial discretization has strong influence on the remaining temporal system dynamics and can even mislead to wrong results if performed insufficiently. The typically large set of ordinary differential equations requires high computing power for dynamic simulation and is ill-suited for model-based controller design, in general.

Another way to analyze PDE (7) is a modal transformation based on the eigenfunctions of PDE (7) fulfilling the homogeneous boundary conditions (9)-(11). The modal transformation leads to an infinite set of ordinary differential equations in modal coordinates describing only the temporal evolution of the eigenfunctions of PDE (7). Thereby, all spatial and temporal properties are preserved and a reduced set of the ODEs can be used for dynamic simulation and controller design.

The eigenfuntions $W_k(r, \theta)$ of PDE (7) can be derived by separation of variables with

$$\Gamma: \quad w(r, \theta, t) = \sum_{k=1}^{\infty} W_k(r, \theta) f_k(t), \tag{13}$$

where the eigenfunctions $W_k(r, \theta)$ describe the spatial characteristics and the modal coefficients $f_k(t)$ describe the time-varying amplitude. At the same time, equation (13) can be used to perform a transformation from modal coordiantes $f_k(t)$ to physcial coordinates $w(r, \theta, t)$ and back, which will be needed for feedback controller design in Section 4.3.

After inserting (13) in the homogeneous PDE (7) with $q(r, \theta) = 0$, an analytical description of the eigefunctions $W_k(r, \theta, t)$ can be found as described in [23] reading

$$\begin{aligned} W_k(r, \theta) = {} & (A_{1k} J_k(\beta r) + A_{2k} Y_k(\beta r) + A_{3k} I_k(\beta r) + A_{4k} K_k(\beta r)) \cos(k\theta) \\ & + (B_{1k} J_k(\beta r) + B_{2k} Y_k(\beta r) + B_{3k} I_k(\beta r) + B_{4k} K_k(\beta r)) \sin(k\theta). \end{aligned} \tag{14}$$

Here, J_k, Y_k, I_k, K_k are Bessel functions and modified Bessel functions of first and second kind. The eigenfunctions fulfill the relation

$$\nabla^4 W_k(r, \theta) = \beta^4 W_k(r, \theta) \tag{15}$$

and are self-adjoint due to the biharmonic operator ∇^4.

After inserting the fundamental solution (14) in the boundary conditions (9)-(11), the free parameters $A_{1k}, \ldots, A_{4k}$ and $B_{1k}, \ldots, B_{4k}$ can be found by computing a non-trivial solution of the resulting homogeneous equations

http://dx.doi.org/10.5772/52726

$$\Lambda_c(\beta_k)\begin{bmatrix} A_{1k} \\ A_{2k} \\ A_{3k} \\ A_{4k} \end{bmatrix} = 0, \quad \Lambda_s(\beta_k)\begin{bmatrix} B_{1k} \\ B_{2k} \\ B_{3k} \\ B_{4k} \end{bmatrix} = 0\,, \tag{16}$$

where $\Lambda_c(\beta)$ and $\Lambda_s(\beta)$ are $[4 \times 4]$ matrices containing linear combinations of Bessel functions depending on the eigenvalue β_k for the cosine and sine parts of $W_k(r,\theta)$. A computation of matrices Λ_c and Λ_s should be performed using computer algebra software since the matrix elements are rather extensive.

where $\Lambda_c(\beta)$ and $\Lambda_s(\beta)$ are $[4 \times 4]$ matrices containing linear combinations of Bessel functions depending on the eigenvalue β_k for the cosine and sine parts of $W_k(r,\theta)$. A computation of matrices Λ_c and Λ_s should be performed using computer algebra software since the matrix elements are rather extensive.

In order to compute a non-trivial solution of the homogeneous equations (16), the parameter β_k needs to determined such that Λ_c and Λ_s contain a non-trivial kernel. This can be achieved by numerically searching for zeros in the determinant of the matrices Λ_c and Λ_s and leads to infinitely many eigenvalues β_k related to the eigenfunction $W_k(r,\theta)$.

In Figure 4, the consine parts of the first 21 analytical eigenfunctions $W_k(r,\theta)$, $k = 1,\ldots,21$ of a deformable mirror with clamped inner radius and free outer radius are shown based on the calculations given before. The eigenfunctions $W_k(r,\theta)$ and eigenvalues β_k were compared with a detailed finite element model of the same mirror and show excellent compliance.

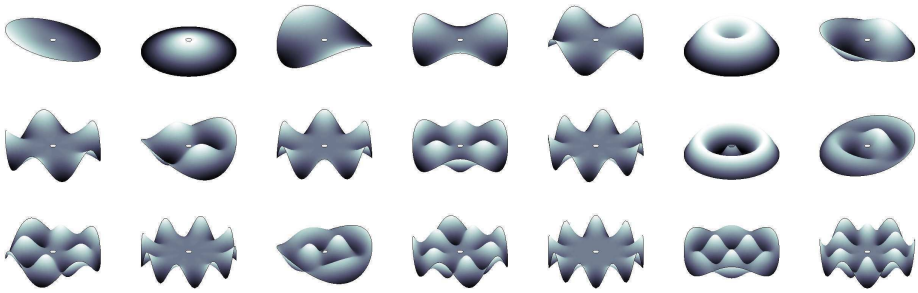

Figure 4. First 21 eigenfunctions of a deformable mirror model (7) with clamped edge boundary conditions (9) at the inner radius r_1 and free edge boundary conditions (11) at the outer radius r_2 ordered by increasing eigenfrequency.

In the following, a modal decomposition of PDE (7) is used to analyze the mirror dynamics and to derive model-based feedforward control commands in modal coordinates. The modal decomposition of (7) is performed by inserting relation (13) in (7) and using property (15) yielding

$$\sum_{k=1}^{\infty}\left(D\beta_k^4 f_k(t)+(\lambda_d+\kappa_d\beta^4)\dot{f}_k(t)+\rho h\ddot{f}_k(t)\right)W_k(r,\theta)=\sum_{m=1}^{M}\frac{u_m(t)}{r_m}\delta(r-r_m)\delta(\theta-\theta_m). \quad (17)$$

A multiplication with any eigenfunction W_j and integration over domain S on both sides gives

$$\iint_S W_j(r,\theta)\sum_{k=1}^{\infty}\left(D\beta_k^4 f_k(t)+(\lambda_d+\kappa_d\beta_k^4)\dot{f}_k(t)+\rho h\ddot{f}_k(t)\right)W_k(r,\theta)\mathrm{d}S = \iint_S W_j(r,\theta)\sum_{m=1}^{M}\frac{u_m(t)}{r_m}\delta(r-r_m)\delta(\theta-\theta_m)\mathrm{d}S. \quad (18)$$

Changing order of summation and integration, using the orthonormality property of the eigenfunctions $W_k(r,\theta)$, and considering the sifting property of the Dirac delta function δ on the right hand side of Equation (18) leads to an infinite set of second order ordinary differential equations

$$\ddot{f}_j(t)+\frac{\lambda_d+\kappa_d\beta_j^4}{\rho h}\dot{f}_j(t)+\frac{D\beta_j^4}{\rho h}f_j(t)=\frac{1}{\rho h}\sum_{m=1}^{M}W_j(r_m,\theta_m)u_m(t)\,, \quad (19)$$
$$f_j(0)=0,\quad \dot{f}_j(0)=0,\qquad j\in\mathbb{N}\,.$$

For each j, the resulting ODE (19) describes the temporal evolution of the corresponding eigenfunction $W_j(r,\theta)$ by the modal coefficient $f_j(t)$. For simplicity, homogeneous initial conditions are assumed describing a flat and steady mirror surface.

Since there is no coupling between different modal coefficients $f_k(t)$ and $f_j(t)$, $j\neq k$, the ODEs (19) can be used for dynamic simulation of a mirror surface described by a specific eigenfunction $W_j(r,\theta)$ or a linear combination of eigenfunctions. Any physically relevant mirror deformation can be decomposed into a linear combination of the orthonormal eigenfunctions $W_k(r,\theta)$ and all relevant dynamic properties of the deformable mirror can be covered with this approach. The decoupled description of the mirror dynamics in modal coordinates (19) allows for simplified system analysis and is the foundation for the following controller design.

Based on the derived normalized eigenfunctions $W_k(r,\theta)$, an analytical solution of the biharmonic equation (7) with initial conditions $w(r,\theta,0)=0$ and $\dot{w}(r,\theta,0)=0$ can be derived in spectral form reading

http://dx.doi.org/10.5772/52726

$$w(r,\theta,t) = \int_{\tau=0}^{t} \underbrace{\sum_{k=1}^{\infty}\sum_{m=1}^{M} \frac{1}{\zeta_k} W_k(r,\theta)\, W_k(r_m,\theta_m) g_k(t-\tau)}_{G(r,\theta,r_m,\theta_m,t-\tau)}\, u_m(\tau)\mathrm{d}\tau, \tag{20}$$

with

$$g_k(t-\tau) = e^{-\frac{t}{2\rho h}\left(\lambda_d+\kappa_d\beta_k^4+\zeta_k\right)} - e^{-\frac{t}{2\rho h}\left(\lambda_d+\kappa_d\beta_k^4-\zeta_k\right)}, \quad \zeta_k = \sqrt{(\lambda_d+\kappa_d\beta_k^4)^2 - 4D\rho h\beta_k^4}\,.$$

Equation (20) can be used to compute the actuator influence functions for any input signal $u_m(\tau)$, $m = 1 \ldots M$. Thereby, not only the resulting static deformation of the mirror can be computed, but also the transient motion of the plate for time-varying input forces.[3] Additionally, relation (20) can be used to compute the frequency responses of a deformable mirror at different actuator locations as shown in Figure 5 for a deformable mirror with clamped inner edge, free outer edge, and co-located force actuators and position sensors.

The infinite sum of eigenfunctions $W_k(r,\theta)$ in Equation (20) can be approximated with a finite k using only a limited number of eigenfunctions. The right number of eigenfunctions can either be driven by a sufficient static coverage of mirror deformations with linear combinations of k eigenfunctions $W_k(r,\theta)$, or by considering a certain number of eigenvalues β_k in order to sufficiently describe the mirror dynamics up to a certain eigenfrequency.

Obviously, the frequency responses shown in Figure 5 reveal essential variations of local mirror dynamics depending on the co-located actuator/sensor position. From a control point of view, this behavior illustrates the difficulty of designing a decentralized controller that can be used for every actuator/sensor pair of the DM.

4. Model-based controller design

In a typical AO system, the requirement of changing the mirror shape within a predefined time T from an initial deformation $\triangle w_1^*$ to a final deformation $\triangle w_2^*$ is derived from the higher-ranking AO control loop (see Figure 6). This control loop runs at a fixed cycle time and sends mirror deformations $\triangle w^*(t)$ to the shape controller in order to correct for measured optical disturbances in the AO system (not shown in Figure 6). The step inputs $\triangle w^*(t)$ for the model-based shape controller in Figure 6 are in general ill-suited for model-based feedforward control and need to be filtered beforehand. The transition time T for changing the mirror shape from its initial shape $\triangle w_1$ to its new desired shape $\triangle w_2$ is assumed to be smaller than the cycle time of the higher-ranking AO control loop. This requirement assures that the closed loop mirror dynamics can be neglected with respect to the higher-ranking AO control loop when designing the AO loop controller.

For model-based shape control of deformable mirrors, the control scheme shown in Figure 6 can be used. It consists of a deformable mirror with multiple inputs $u = \begin{bmatrix} u_1 & u_2 & \ldots & u_M \end{bmatrix}$

[3] In Equation (20) and for the following analysis, it is assumed that the eigenfunctions $W_k(r,\theta)$ are normalized with respect to the L_2 scalar product $\langle W_k, W_k \rangle = 1$.

(force actuators), multiple outputs $y = \begin{bmatrix} y_1 \; y_2 \; \dots \; y_M \end{bmatrix}$ (position sensors), and an underlying shape controller in a two-degree-of-freedom control structure. The control structure contains an online trajectory generator Σ^*_{traj}, a static and a dynamic model-based feedforward controller Σ^{-1}_{stat} and Σ^{-1}_{dyn}, and a model-based feedback controller Σ_{crtl}.

There are two control objectives adressed by the control structure shown in Figure 6. One is achieving good tracking performance along a spatio-temporal trajectory y_d describing the evolution of the mirror shape from an initial shape $\triangle w^*_1$ to a new commanded mirror shape $\triangle w^*_2$ in a predefined time T. The second control objective is the stabilization of the deformable mirror shell by feedback control Σ_{ctrl} along the generated trajectory y_d and in its final position $\triangle w^*_2$ with respect to external disturbances and model uncertainties.

4.1. Design of the trajectory generator Σ^*_{traj}

The trajectory generator Σ^*_{traj} generates a continuously differentiable output signal y_d that reaches its final value $\triangle w^*_2$ within a fixed transition time T. In Figure 7, the piecewise constant input $\triangle w^*$ and filtered output signal y_d are illustrated for a single set-point change. Since the deformable mirror consists of many inputs and outputs, the signals $\triangle w^*$ and y_d are vectorial variables containing deformation values either in modal or physical coordinates. The choice of units can be driven by the higher-ranking AO control loop and is only of minor importance for the following section.[4]

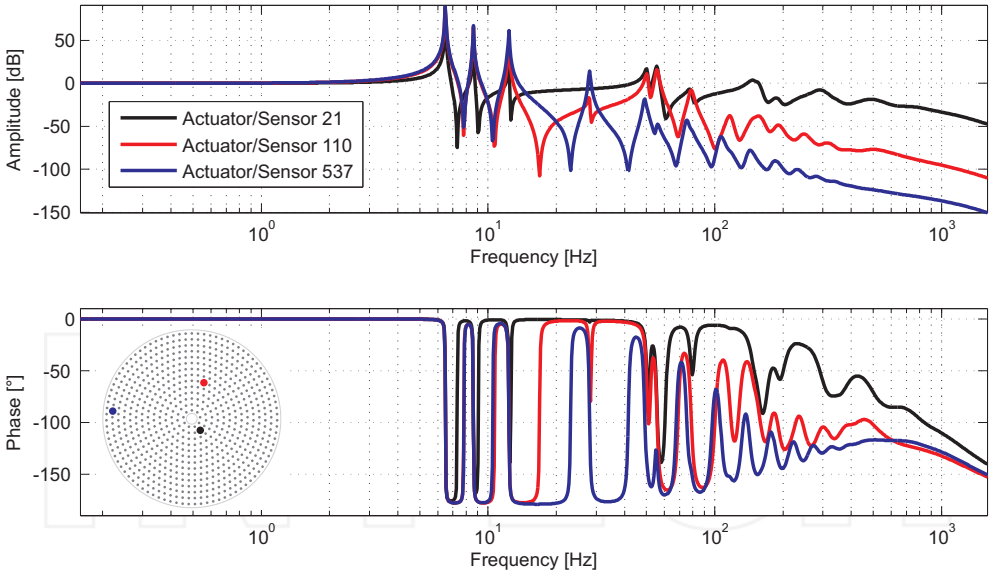

Figure 5. Bode diagram of the analytical local transfer functions of a deformable mirror at different co-located actuator/sensor positions (normalized).

[4] A linear forward or backward transformation can be used to transform physical coordinates $w(r, \theta, t)$ into modal coordinates $f_k(t)$ using the orthonormal eigenfunctions $W_k(r, \theta)$ in 13.

http://dx.doi.org/10.5772/52726

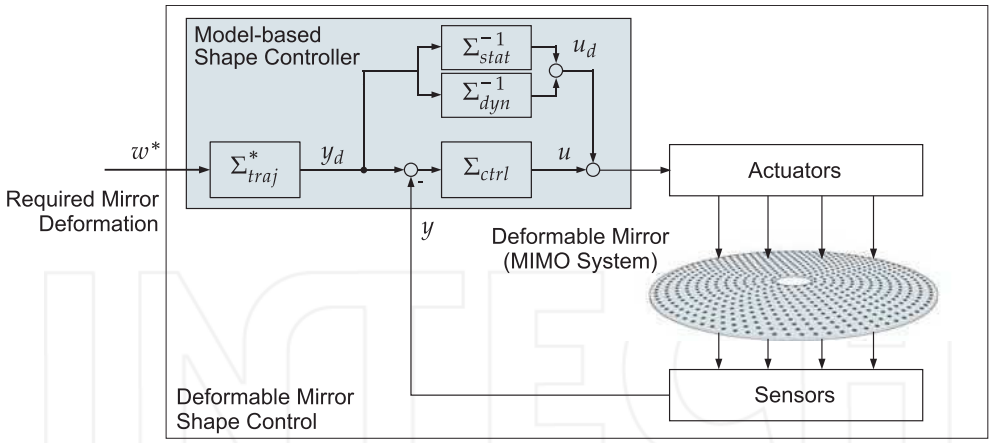

Figure 6. Two-degree-of-freedom structure for shape control of deformable mirrors modeled as a multi-input multi-ouput (MIMO) system with co-located non-contacting force actuators and position sensors consisting of a trajectory generator Σ_{traj}^*, a static and a dynamic model-based feedforward controller Σ_{stat}^{-1} and Σ_{dyn}^{-1}, and a feedback controller Σ_{ctrl}.

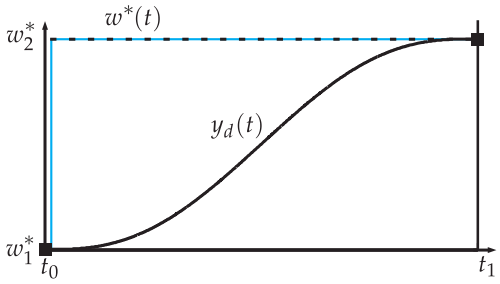

Figure 7. Illustration of a general input signal $\triangle w^*(t)$ and the resulting output signal $y_d(t)$ of the trajectory generator Σ_{traj}^* within a fixed transition time $T = t_2 - t_1$.

There are several ways to generate the output signal y_d based on the step input $\triangle w^*$, e.g. finite impuls response (FIR) filters, sigmoid basis functions, or segmented polynomials. In [20] and [21] a detailed introduction to this topic is given with respect to control of deformable mirrors. A more general and comprehensive discussion on trajectory generation can be found in [45]. Here, a polynomial ansatz function is used to generate the output signal y_d for simplicity.

Depending on the required smoothness of y_d, the reference trajectory y_d is described by

$$\Sigma_{traj}^*: \quad y_d(t) = \triangle w_1^* + (\triangle w_2^* - \triangle w_1^*)\kappa(t - t_0), \quad t \in [t_0, t_1],\ t_1 = t_0 + T, \tag{21}$$

with

$$\kappa(t) = \begin{cases} 0 \quad \text{if } t \leq (t_1 - t_0) \\ \frac{(2n+1)!}{n!(t_1-t_0)^{2n+1}} \sum_{i=0}^{n} \frac{(-1)^{n-i}}{i!(n-i)!(2n-i+1)} (t_1 - t_0)^i t^{2n-i+1} \\ \qquad\qquad\qquad\qquad \text{if } 0 \leq t \leq (t_1 - t_0) \\ 1 \quad \text{if } t \geq (t_1 - t_0). \end{cases} \tag{22}$$

The transition time T must be chosen shorter than the higher-ranking AO loop cycle time but long enough to comply with input constraints of the force actuators. The shorter the transition time T is chosen, the higher the required input forces u will be in order to drive the mirror from one deformation to another one. The required smoothness of the trajectory y_d depends on the parameter n and should be chosen $n \geq 3$ in order to be able to apply the model-based feedforward control scheme presented in the next section.

4.2. Design of the model-based feedforward controller Σ_{stat}^{-1} and Σ_{dyn}^{-1}

The basic idea of model-based feedforward control is the application of a desired input signal $u_d(t)$ such that the system response $y(t)$ follows a desired output behavior $y_d(t)$ (see Figure 6). The transient deformation of the deformable mirror is described by the planned output $y_d(t)$ and leads to a new steady shape $\triangle w_2^*$ using an inverse model of the system dynamics of the DM. The design of the desired response $y_d(t)$ is performed in the on-line trajectory generator Σ_{traj}^* described in Section 4.1.

As shown in Figure 6, the feedforward control concept is seperated into a static and a dynamic component Σ_{stat}^{-1} and Σ_{dyn}^{-1}. The feedforward component Σ_{dyn}^{-1} contains the dynamic inverse of the relevant mirror dynamics and is based on the modal system dynamics (19) reading

$$\ddot{f}_j(t) + \underbrace{\frac{\lambda_d + \kappa_d \beta_j^4}{\rho h}}_{2d_j\omega_j} \dot{f}_j(t) + \underbrace{\frac{D\beta_j^4}{\rho h}}_{\omega_j^2} f_j(t) = \underbrace{\frac{1}{\rho h} \sum_{m=1}^{M} W_j(r_m, \theta_m)}_{b_j} u_m(t)\,, \tag{23}$$

By transforming the desired output behavior y_d into modal coordinates $f_j(t)$ with relation (13), the left hand side of Equation (23) is fully defined by the desired modal output behavior $f_k(t)$ and the first two time derivatives of $f_k(t)$. Thus, the dynamic part of the required input command u_d achieving the planned output behavior $f_k(t)$ can be computed as

$$\Sigma_{dyn}^{-1}: \quad u_m^{dyn}(t) = \frac{1}{b_j} \left(\ddot{f}_j(t) + 2d_j\omega_j \dot{f}_j(t) + \omega_j^2 f_j(t) \right) \tag{24}$$

for a limited number of $j = 1, \ldots, N$ dynamic eigenmodes. Since viscous and Rayleigh damping typically increase for higher order eigenmodes, it is not necessary to consider all eigenmodes in the dynamic feedforward component Σ_{dyn}^{-1}. Instead, it is sufficient to

http://dx.doi.org/10.5772/52726

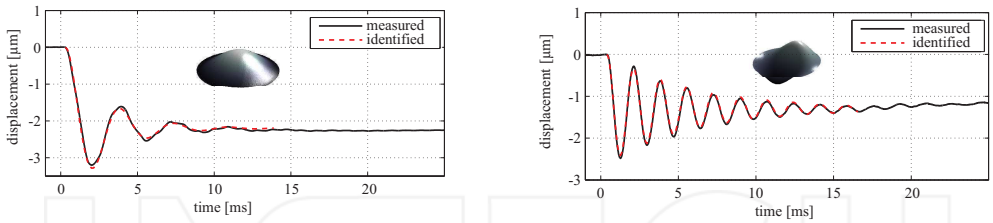

Figure 8. Measured step responses of the first and second eigenfunctions of an Alpao DM88 deformable membrane mirror without feedforward control showing a settling time above 5-10 ms

consider only the static components of the inverse system dynamics (23) and compute a static command $u_m^{stat}(t)$ as

$$\Sigma_{stat}^{-1}: \quad u_m^{stat}(t) = \frac{1}{b_j}\left(\omega_j^2 f_j(t)\right). \tag{25}$$

Afterwards, the final feedforward command u_d can be computed as

$$u_d(t) = u^{dyn}(t) + u^{stat}(t). \tag{26}$$

Regarding the computational complexity, in [20] is shown that the computational demands of feedforward control scale quadratically with the number of system inputs and outputs. However, since the control signal only needs to be computed with the frequency of the outer AO-loop (e.g. 1 kHz in modern astronomical AO systems), there are currently no burdens for a practical implementation in existing systems.

In Figure 8 and Figure 9 measurement results of a setpoint change without and with feedforward control for an Alpao deformable mirror with 88 voice coil actuators is shown. In the experiment, the first two eigenfunctions of the deformable mirror are excited by a modal step input (spatially distributed step command for all 88 actuators at the same time) and a model-based feedforward control input u_d (spatially distributed time-varying signal for all 88 actuators) based on a polynomial of degree $n = 3$ and identified modal damping and eigenfrequencies in (24). Clearly, overshoot and settling time of the feedforward scheme show considerable improvements to a pure step command. Thereby, no feedback control is implemented at this stage and only the trajectory generator Σ_{traj}^{*} and the inverse modal system dynamics Σ_{dyn}^{-1} are used to generate the control command $u = u_d$ (see Figure 6).

Feedforward control of deformable membrane mirrors has also been demonstrated at the P45 adaptive secondary prototype of the Large Binocular Telescope adaptive secondary mirror in [21] with similar results. In addition, a flatness based feedforward control is proposed therein in case of zero dynamics in the differential equation (19).

In order to further improve the system response to feedforward control and in order to add additional disturbance rejection capabilities to the DM control scheme, a model-based

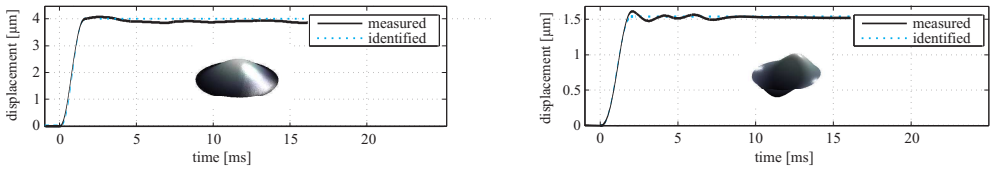

Figure 9. Measured responses of the first and second eigenfunctions of an Alpao DM88 deformable membrane mirror with feedforward control showing a settling time of 2 ms

feedback controller is designed in the following section and its sparse structure for local implementation is discussed.

4.3. Design of the model-based feedback controller Σ_{ctrl}

Feedforward control combined with suitable trajectory generation methods improve the input output behavior of deformable mirrors significantly. However, in case of model uncertainties or external disturbances, the tracking performance shown in Figure 9 can be affected considerably. For this reason, active position feedback is integrated in modern deformable mirrors measuring the local mirror position at each actuator generating an error compensation command.

Due to the spatially distributed mirror dynamics, global instead of local position control of deformable mirrors is the most promising solution for error compensation and disturbance rejection. However, the computational complexity for high order spatial control of the deformable element typically exceeds available computing power. For this reason, existing deformable membrane mirrors for large telescopes incorporate local feedback instead of global feedback control and neglect some of the global dynamics of the deformable mirror [10, 13, 14, 46–48]. As a side effect, dynamic coupling of separately controlled actuators through the deformable membrane can lead to instability of the individually stable loops and draws the need for carefully designing the control parameters of the local feedback loops.

In the following, an advanced control concept for position control of large deformable mirrors is derived based on the detailed dynamical model of the deformable mirror (7), suitable boundary conditions (9)-(12), and its represenation in modal coordinates (23). The presented controller design differs from existing ones since it incorporates a detailed mirror model and comprises a decentralized structure at the same time.

For feedback controller design, the first N relevant modal differential equations (23) are combined in state space form as

$$\begin{aligned} \dot{x}(t) &= Ax(t) + Bu(t) \\ y(t) &= Cx(t), \end{aligned} \tag{27}$$

with $x(t) = \left[f_1(t)\ f_2(t)\ \dots\ f_N(t)\ \dot{f}_1\ \dot{f}_2\ \dots\ \dot{f}_N(t) \right]^T$ and system matrices

$$A = \begin{bmatrix} 0 & 0 & 0 & \dots & 0 & 1 & 0 & 0 & \dots & 0 \\ \frac{D\beta_1^4}{\rho h} & 0 & 0 & \dots & 0 & \frac{\lambda_d+\kappa_d\beta_1^4}{\rho h} & 0 & 0 & \dots & 0 \\ 0 & 0 & 0 & \dots & 0 & 0 & 1 & 0 & \dots & 0 \\ 0 & \frac{D\beta_2^4}{\rho h} & 0 & \dots & 0 & 0 & \frac{\lambda_d+\kappa_d\beta_2^4}{\rho h} & 0 & \dots & 0 \\ 0 & 0 & 0 & \dots & 0 & 0 & 0 & 1 & \dots & 0 \\ 0 & 0 & \frac{D\beta_3^4}{\rho h} & \dots & 0 & 0 & 0 & \frac{\lambda_d+\kappa_d\beta_3^4}{\rho h} & \dots & 0 \\ \vdots & \vdots & \vdots & \ddots & \vdots & \vdots & \vdots & \vdots & \ddots & \vdots \\ 0 & 0 & 0 & \dots & 0 & 0 & 0 & 0 & \dots & 1 \\ 0 & 0 & 0 & \dots & \frac{D\beta_N^4}{\rho h} & 0 & 0 & 0 & \dots & \frac{\lambda_d+\kappa_d\beta_N^4}{\rho h} \end{bmatrix}, \tag{28}$$

$$B = \frac{1}{\rho h} \begin{bmatrix} W_1(r_1,\theta_1) & \dots & W_1(r_M,\theta_M) \\ W_2(r_1,\theta_1) & \dots & W_2(r_M,\theta_M) \\ \vdots & \dots & \vdots \\ W_N(r_1,\theta_1) & \dots & W_N(r_M,\theta_M) \\ 0 & \dots & 0 \\ \vdots & \ddots & \vdots \\ 0 & \dots & 0 \end{bmatrix}, \tag{29}$$

$$C = \begin{bmatrix} W_1(r_1,\theta_1) & \dots & W_N(r_1,\theta_1) & 0 \dots 0 \\ W_1(r_2,\theta_2) & \dots & W_N(r_2,\theta_2) & 0 \dots 0 \\ \vdots & \ddots & \vdots & \vdots \ddots \vdots \\ W_1(r_M,\theta_M) & \dots & W_N(r_M,\theta_M) & 0 \dots 0 \end{bmatrix}. \tag{30}$$

A global multi-input multi-ouput linear quadratic regulator is designed for controlling the system along the planned trajectory $x_d(t)$ using the optimization criterion

$$J = \int_0^\infty \left(x(t) - x_d(t)\right)^T Q \left(x(t) - x_d(t)\right) + u(t)^T R u(t) \mathrm{d}t, \tag{31}$$

with Q being a positive definite and R being a positive semi-definite matrix. Assuming the pair (A, Q) is observable, a minimization of (31) can be achieved by the state feedback

$$\Sigma_{ctrl}: \quad u(t) = -K\left(x(t) - x_d(t)\right) \tag{32}$$

with

$$K = R^{-1}B^T P\,. \tag{33}$$

The matrix P is the symmetric, positive definite solution of the matrix Ricatti equation

$$A^T P + PA - PBR^{-1}B^T P + Q = 0 \tag{34}$$

and can be computed efficiently in modern mathematical computing languages (e.g. Matlab). By choosing $Q = C^T c_1 C$ and $R = Ic_2$, the optimization criterion for a deformable mirror with M inputs and M outputs simplifies to

$$J = \int_0^\infty \sum_{m=1}^{M} \left(c_1 y_m^2(t) + c_2 u_m^2(t) \right) \mathrm{d}t \tag{35}$$

and a decentralized controller can be computed via (33) and (34). The particular choice of weight matrices Q and R is the essential step for a decentralized controller in the LQR framework. The coefficients c_1 and c_2 are used to tune the closed loop disturbance rejection and robustness until certain settling time and gain margins are achieved.

Since the controller K requires modal signals $x(t)$, a feedback controller K_p in physical coordinates can be computed performing an inverse modal transformation Γ^{-1} from (13) reading

$$K_p = \Gamma^{-1} K\,. \tag{36}$$

with the feedback law

$$u(t) = -K_p \left(\left[\, x(t) \;\; \dot{x}(t) \, \right]^T - \left[\, x_d(t) \;\; \dot{x}_d(t) \, \right]^T \right) . \tag{37}$$

For comparison, the closed loop transfer functions at selected co-located actuator/sensor locations with active LQ feedback are shown in Figure 10. In comparison to the open loop transfer functions in Figure 5, all relevant low and high frequency resonances are fully damped in the closed loop case and the resulting bandwidth of the deformable mirror exceeds 1 kHz. In order to tune the resulting performance for existing deformable mirrors, a variation of parameters c_1 and c_2 can be performed easily in practice.

http://dx.doi.org/10.5772/52726

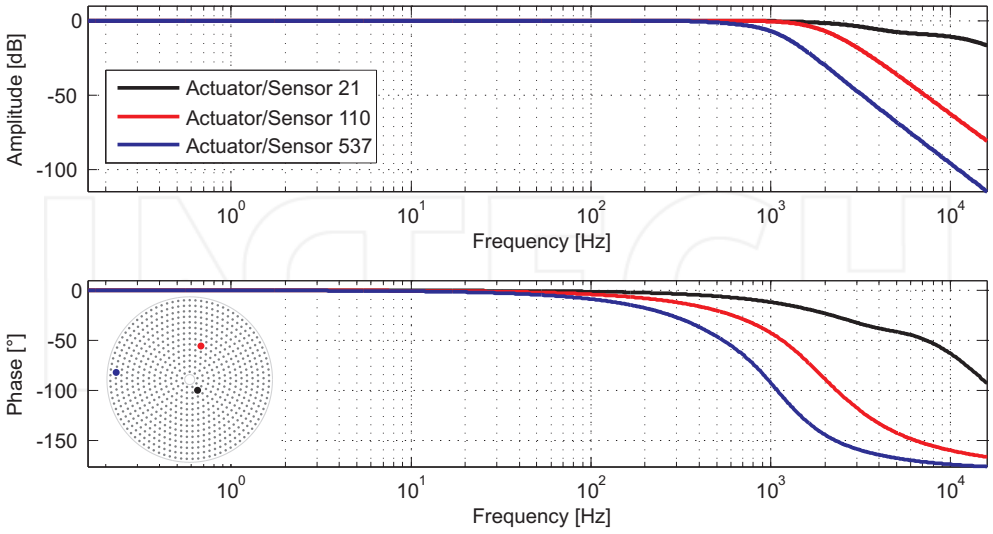

Figure 10. Bode diagram of the closed loop local transfer functions at different co-located actuator/sensor positions using decentralized LQR control (normalized).

In Equation (37), it can be seen that the columns of K_p contain information about how much displacement and velocity feedback is required for a certain actuator in vector $u(t)$. A visualization of entries in K_p shown in Figure 11 reveals that only a limited amount of displacement and velocity information around each actuator is needed to compute the feedback signal $u(t)$. This property can be used to truncate the spatial extension of the global LQ regulator and leads to a decentralized control scheme.

For a deformable mirror with 672 actuators and sensors, the corresponding normalized entries of the state feedback matrix K_p are visualized in Figure 11. Clearly, a choice of $c_1 = 1000$ and $c_2 = 0.1$ results in a fully decentralized structure of K_p. Comparing the position and velocity feedback entries of K_p in Figure 11, dynamic effects of boundary conditions and actuator position can be seen. Consequently, a model-free decentralized control law for all actuators seems unreasonable and the suggested linear quadratic regulator approach should be considered when designing deformable mirror controllers for astronomical telescopes or comparible application areas. Depending on the truncation area, the computational demands of this control concept scale linearly with the number of actuators and show the applicability of global LQ - control for shape control of large deformable mirrors in general.

Although controller K requires full state information, the state feedback controller can be transformed into an output feedback controller using loop transfer recovery (LTR) and results in an output controller Σ_{ctrl} as shown in Figure 6. The ouput controller can be implemented on existing hardware as a finite impulse response (FIR) filter for each actuator/sensor pair where the number of filter coefficients is mainly driven by the acceptable approximation error of the loop transfer recovery approach.

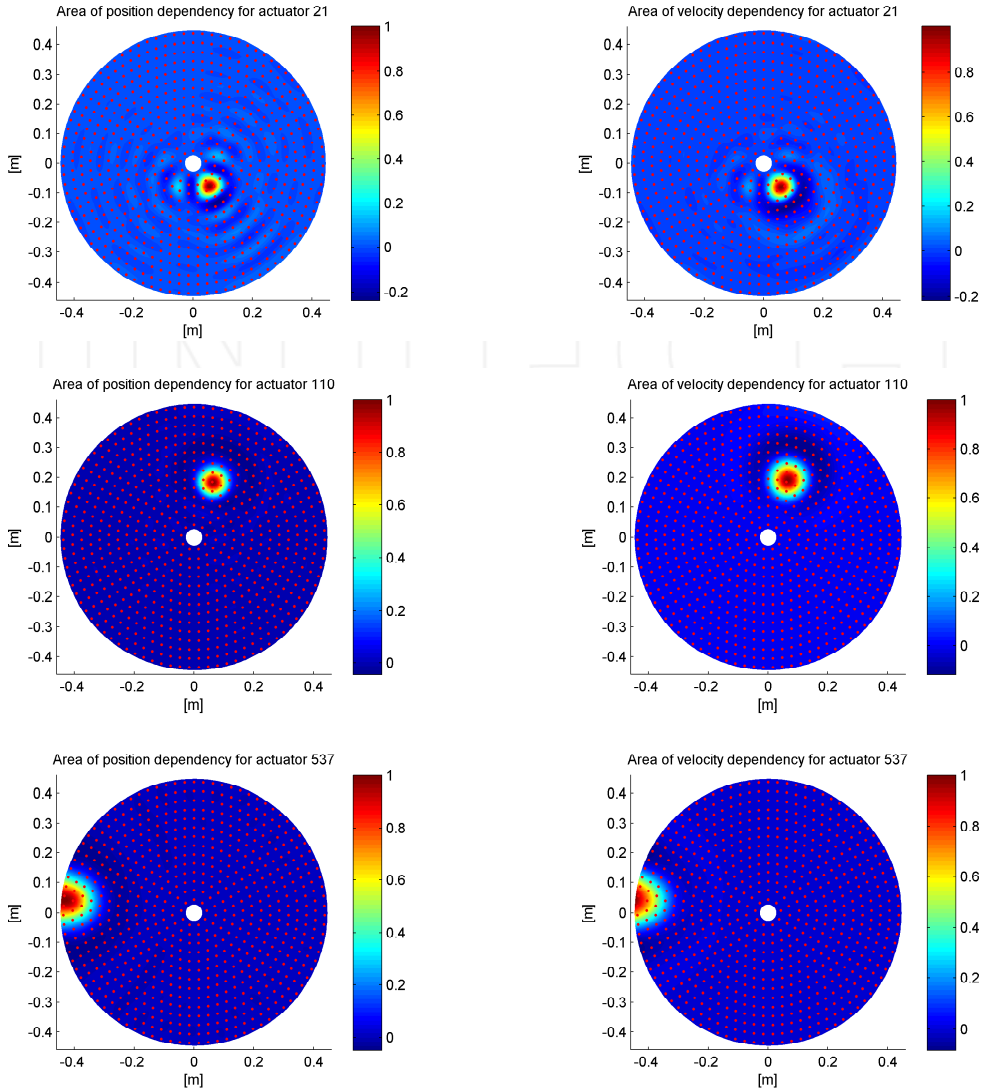

Figure 11. Vislization of the decentralized spatial structure of the feedback matrix K_p for selected co-located actuator/sensor pairs.

5. Conclusion

Control of deformable mirrors becomes relevant when the mirror dynamics are slower or equivalent with the dynamics of optical disturbances that shall be compensated by the deformable mirror. Active shape control of deformable mirrors can thereby increase the mirrors bandwidth and make it suitable for the AO task, again. When designing a model-based shape controller for a deformable mirror in a two-degree-of-freedom control

structure, there are three components to be considered (see Figure 6): First, a trajectory generator Σ_{traj} providing continuous reference trajectories y_d for fast setpoint changes of the DM shape. Second, a static and dynamic feedforward controller Σ_{stat}^{-1} and Σ_{dyn}^{-1} generating control commands for driving the mirror along the precomputed trajectory based on inverse system dynamics. Finally, a feedback controller Σ_{ctrl} responsible for compensation of model errors in the feedforward part and rejection of external disturbances.

In this chapter, model-based design steps for all three components were shown supported by experimental and simulation results. The key for decentralized controller design is the right choice of weighting matrices Q and R in the LQR framework. Followed by a loop transfer recovery approach, the state feedback controller can be transformed into an ouput feedback controller that can be implemented as FIR filters on existing hardware.

Future astronomical optical telescopes, e.g. the European Extremely Large Telescope (E-ELT) or the Giant Magellan Telescope (GMT), will include deformable mirrors with many thousand actuators and position sensors. Due to the inherent slow dynamics of the large deformable mirror shells, active shape control of these elements is inevitable. Model-based shape control in a two-degree-of-freedom structure can greatly improve the performance of these elements and should be considered for comparible AO systems with high performance requirements, also.

Acknowledgements

The author would like to acknowledge the support by INAF and the Osservatorio Astrofisico di Arcetri in particular, providing finite element data of the LBT ASM and detailed insight into current deformable mirror control schemes. This work was supported by the DFG under grant SA-847/10-1 and OS-111/29-1 and by the Carl Zeiss AG.

Author details

Thomas Ruppel

Carl Zeiss AG, Corporate Research and Technology, Optronics Systems, Jena, Germany

References

[1] Edward P. Wallner. Optimal wave-front correction using slope measurements. *J. Opt. Soc. Am.*, 73(12):1771–1776, 1983.

[2] R.K. Tyson. *Adaptive optics engineering handbook*. CRC, 2000.

[3] B.W. Frazier and R.K. Tyson. Robust control of an adaptive optics system. In *System Theory, 2002. Proceedings of the Thirty-Fourth Southeastern Symposium on*, pages 293–296, 2002.

[4] H. M. Martin, G. Brusa Zappellini, B. Cuerden, S. M. Miller, A. Riccardi, and B. K. Smith. Deformable secondary mirrors for the LBT adaptive optics system. In Domenico Ellerbroek, Brent L.; Bonaccini Calia, editor, *Advances in Adaptive Optics II*, volume 6272 of *Proc. SPIE*, page 0U, July 2006.

[5] M.J. Booth, M.A.A. Neil, R. Juškaitis, and T. Wilson. Adaptive aberration correction in a confocal microscope. *Proceedings of the National Academy of Sciences of the United States of America*, 99(9):5788, 2002.

[6] M.J. Booth. Adaptive optics in microscopy. *Philosophical Transactions of the Royal Society A: Mathematical, Physical and Engineering Sciences*, 365(1861):2829, 2007.

[7] Junzhong Liang, David R. Williams, and Donald T. Miller. Supernormal vision and high-resolution retinal imaging through adaptive optics. *J. Opt. Soc. Am. A*, 14(11):2884–2892, 11 1997.

[8] Austin Roorda, Fernando Romero-Borja, III William Donnelly, Hope Queener, Thomas Hebert, and Melanie Campbell. Adaptive optics scanning laser ophthalmoscopy. *Opt. Express*, 10(9):405–412, 05 2002.

[9] Daniel C. Gray, William Merigan, Jessica I. Wolfing, Bernard P. Gee, Jason Porter, Alfredo Dubra, Ted H. Twietmeyer, Kamran Ahamd, Remy Tumbar, Fred Reinholz, and David R. Williams. In vivo fluorescence imaging of primate retinal ganglion cells and retinal pigment epithelial cells. *Opt. Express*, 14(16):7144–7158, Aug 2006.

[10] D. G. Bruns, D. G. Sandler, B. Martin, and G. Brusa. Design and prototype tests of an adaptive secondary mirror for the new 6.5-m single-mirror MMT. *Society of Photo-Optical Instrumentation Engineers (SPIE) Conference Series*, 2534:130–133, 08 1995.

[11] G. Brusa, A. Riccardi, S. Ragland, S. Esposito, C. del Vecchio, L. Fini, P. Stefanini, V. Biliotti, P. Ranfagni, P. Salinari, D. Gallieni, R. Biasi, P. Mantegazza, G. Sciocco, G. Noviello, and S. Invernizzi. Adaptive secondary P30 prototype: laboratory results. In D. Bonaccini and R. K. Tyson, editors, *Adaptive Optical System Technologies*, volume 3353 of *Society of Photo-Optical Instrumentation Engineers (SPIE) Conference Series*, pages 764–775, September 1998.

[12] A. Riccardi, G. Brusa, P. Salinari, D. Gallieni, R. Biasi, M. Andrighettoni, and H.M. Martin. Adaptive secondary mirrors for the large binocular telescope. *Adaptive Optical System Technologies II*, 4839(1):721–732, 2003.

[13] R. Arsenault, R. Biasi, D. Gallieni, A. Riccardi, P. Lazzarini, N. Hubin, E. Fedrigo, R. Donaldson, S. Oberti, S. Stroebele, R. Conzelmann, and M. Duchateau. A deformable secondary mirror for the VLT. In *Society of Photo-Optical Instrumentation Engineers (SPIE) Conference Series*, volume 6272 of *Society of Photo-Optical Instrumentation Engineers (SPIE) Conference Series*, July 2006.

[14] A. Riccardi, G. Brusa, P. Salinari, S. Busoni, O. Lardiere, P. Ranfagni, D. Gallieni, R. Biasi, M. Andrighettoni, S. Miller, and P. Mantegazza. Adaptive secondary mirrors for the Large binocular telescope. In R. K. Tyson & M. Lloyd-Hart, editor, *Society of Photo-Optical Instrumentation Engineers (SPIE) Conference Series*, volume 5169 of *Presented at the Society of Photo-Optical Instrumentation Engineers (SPIE) Conference*, pages 159–168, December 2003.

[15] Roberto Biasi, Mario Andrighettoni, Daniele Veronese, Valdemaro Biliotti, Luca Fini, Armando Riccardi, Paolo Mantegazza, and Daniele Gallieni. Lbt adaptive secondary electronics. In Peter L. Wizinowich and Domenico Bonaccini, editors, *SPIE*, volume 4839, pages 772–782, 2003.

[16] G. Brusa, A. Riccardi, P. Salinari, F. P. Wildi, M. Lloyd-Hart, H. M. Martin, R. Allen, D. Fisher, D. L. Miller, R. Biasi, D. Gallieni, and F. Zocchi. MMT adaptive secondary: performance evaluation and field testing. In *Adaptive Optical System Technologies II. Edited by Wizinowich, Peter L.; Bonaccini, Domenico*, volume 4839 of *Society of Photo-Optical Instrumentation Engineers (SPIE) Conference Series*, pages 691–702, February 2003.

[17] DW Miller and SCO Grocott. Robust control of the multiple mirror telescope adaptive secondary mirror. *Optical Engineering*, 38(8):1276 – 1287, 1999.

[18] C. R. Vogel and Q. Yang. Modeling and open-loop control of point-actuatied, continuous facesheet deformable mirrors. In *Society of Photo-Optical Instrumentation Engineers (SPIE) Conference Series*, volume 6272 of *Society of Photo-Optical Instrumentation Engineers (SPIE) Conference Series*, July 2006.

[19] Lucie Baudouin, Christophe Prieur, Fabien Guignard, and Denis Arzelier. Robust control of a bimorph mirror for adaptive optics systems. *Appl. Opt.*, 47(20):3637–3645, 2008.

[20] Thomas Ruppel, Michael Lloyd-Hart, Daniela Zanotti, and Oliver Sawodny. Modal trajectory generation for adaptive secondary mirrors in astronomical adaptive optics. In *Proc. IEEE International Conference on Automation Science and Engineering CASE 2007*, pages 430–435, 9 2007.

[21] T. Ruppel, W. Osten, and O. Sawodny. Model-based feedforward control of large deformable mirrors. *European Journal of Control*, 17(3):261–272, 2011.

[22] T. Ruppel, S. Dong, F. Rooms, W. Osten, and O. Sawodny. Feedforward control of deformable membrane mirrors for adaptive optics. *Transactions on Control Systems Technology*, Accepted for Publication, 2011.

[23] L. Meirovitch. *Analytical methods in vibration*. New York, NY.: The Mcmillan Company, 1967.

[24] Ronald P. Grosso and Martin Yellin. The membrane mirror as an adaptive optical element. *J. Opt. Soc. Am.*, 67(3):399–406, 03 1977.

[25] Luc Arnold. Optimized axial support topologies for thin telescope mirrors. *Optical Engineering*, 34(2):567–574, 1995.

[26] S. K. Ravensbergen, R. F. H. M. Hamelinck, P. C. J. N. Rosielle, and M. Steinbuch. Deformable mirrors: design fundamentals for force actuation of continuous facesheets. In Richard A. Carreras, Troy A. Rhoadarmer, and David C. Dayton, editors, *Proceedings of the SPIE*, volume 7466, page 74660G. SPIE, 2009.

[27] Frederick Bloom and Douglas Coffin. *Handbook of thin plate buckling and postbuckling*. Chapman & Hall/CRC, Boca Raton, FL, 2001.

[28] J Juillard and E Colinet. Modelling of nonlinear circular plates using modal analysis: simulation and model validation. *Journal of Micromechanics and Microengineering*, 16(2):448, 2006.

[29] M. Amabili. *Nonlinear vibrations and stability of shells and plates*. Cambridge University Press, Cambridge and New York, 2008.

[30] J.N. Reddy. *An introduction to the finite element method*, volume 2. McGraw-Hill New York, 1993.

[31] U.F. Meißner and A. Maurial. *Die Methode der finiten Elemente*. Springer Verlag, 2000.

[32] S. E. Winters, J. H. Chung, and S. A. Velinsky. Modeling and control of a deformable mirror. *Journal of Dynamic Systems, Measurement, and Control*, 124(2):297–302, 2002.

[33] C. del Vecchio. Supporting a magnetically levitated very thin meniscus for an adaptive secondary mirror: summary of finite-element analyses [3126-49]. In R. K. Tyson & R. Q. Fugate, editor, *Society of Photo-Optical Instrumentation Engineers (SPIE) Conference Series*, volume 3126 of *Presented at the Society of Photo-Optical Instrumentation Engineers (SPIE) Conference*, pages 397–+, October 1997.

[34] Sven Verpoort and Ulrich Wittrock. Actuator patterns for unimorph and bimorph deformable mirrors. *Appl. Opt.*, 49(31):G37–G46, 11 2010.

[35] Mauro Manetti, Marco Morandini, and Paolo Mantegazza. High precision massive shape control of magnetically levitated adaptive mirrors. *Control Engineering Practice*, 18(12):1386 – 1398, 2010.

[36] G. Agapito, S. Baldi, G. Battistelli, D. Mari, E. Mosca, and A. Riccardi. Automatic tuning of the internal position control of an adaptive secondary mirror. *European Journal of Control*, 17(3):273–289, 2011. Anglais.

[37] R.K. Tyson and B.W. Frazier. *Field guide to adaptive optics*. SPIE Press, 2004.

[38] K. Bush, D. German, B. Klemme, A. Marrs, and M. Schoen. Electrostatic membrane deformable mirror wavefront control systems: design and analysis. In J. D. Gonglewski, M. T. Gruneisen, & M. K. Giles, editor, *Society of Photo-Optical Instrumentation Engineers (SPIE) Conference Series*, volume 5553 of *Presented at the Society of Photo-Optical Instrumentation Engineers (SPIE) Conference*, pages 28–38, October 2004.

[39] E. Scott Claflin and Noah Bareket. Configuring an electrostatic membrane mirror by least-squares fitting with analytically derived influence functions. *J. Opt. Soc. Am. A*, 3(11):1833–1839, 1986.

[40] Arthur Menikoff. Actuator influence functions of active mirrors. *Appl. Opt.*, 30(7):833–838, 1991.

[41] K.F. Graff. *Wave motion in elastic solids*. Dover Pubns, 1991.

[42] E. Cerda and L. Mahadevan. Geometry and Physics of Wrinkling. *Physical Review Letters*, 90(7):074302–+, February 2003.

[43] V.Z. Vlasov. *Allgemeine Schalentheorie und ihre Anwendung in der Technik*. Akademie-Verlag, 1958.

[44] R. Hamelinck, N. Rosielle, P. Kappelhof, B. Snijders, and M. Steinbuch. A large adaptive deformable membrane mirror with high actuator density. *Society of Photo-Optical Instrumentation Engineers (SPIE) Conference Series*, 5490:1482–1492, October 2004.

[45] Steven Fortune and Gordon Wilfong. *Planning constrained motion*. ACM, New York, NY, USA, 1988.

[46] G. Brusa, A. Riccardi, V. Biliotti, C. del Vecchio, P. Salinari, P. Stefanini, P. Mantegazza, R. Biasi, M. Andrighettoni, C. Franchini, and D. Gallieni. Adaptive secondary mirror for the 6.5-m conversion of the Multiple Mirror Telescope: first laboratory testing results. In R. K. Tyson & R. Q. Fugate, editor, *Society of Photo-Optical Instrumentation Engineers (SPIE) Conference Series*, volume 3762 of *Presented at the Society of Photo-Optical Instrumentation Engineers (SPIE) Conference*, pages 38–49, September 1999.

[47] F. P. Wildi, G. Brusa, A. Riccardi, M. Lloyd-Hart, H. M. Martin, and L. M. Close. Towards first light of the 6.5m MMT adaptive optics system with deformable secondary mirror. In *Adaptive Optical System Technologies II. Edited by Wizinowich, Peter L.; Bonaccini, Domenico*, volume 4839 of *Proceedings of the SPIE*, pages 155–163, 02 2003.

[48] Gallieni, D., Tintori, M., Mantegazza, M., Anaclerio, E., Crimella, L., Acerboni, M., Biasi, R., Angerer, G., Andrigettoni, M., Merler, A., Veronese, D., Carel, J-L, Marque, G., Molinari, E., Tresoldi, D., Toso, G., Spanó, P., Riva, M., Mazzoleni, R., Riccardi, A., Mantegazza, P., Manetti, M., Morandini, M., Vernet, E., Hubin, N., Jochum, L., Madec, P., Dimmler, M., and Koch, F. Voice-coil technology for the e-elt m4 adaptive unit. In *1st AO4ELT conference - Adaptive Optics for Extremely Large Telescopes*, page 06002, 2010.

INTECH